Black phosphorus frequency mixer for infrared optoelectronic signal processing

Cite as: APL Photonics 4, 034502 (2019); doi: 10.1063/1.5046732
Submitted: 30 June 2018 • Accepted: 23 October 2018 •
Published Online: 11 December 2018

Ryan J. Suess,[1,2,a)] Joseph D. Hart,[1,3] Edward Leong,[1,2] Martin Mittendorff,[1,4,a)] and Thomas E. Murphy[1,2]

AFFILIATIONS

[1] Institute for Research in Electronics and Applied Physics, University of Maryland, College Park, Maryland 20742, USA
[2] Department of Electrical and Computer Engineering, University of Maryland, College Park, Maryland 20742, USA
[3] Physics Department, University of Maryland, College Park, Maryland 20742, USA
[4] Fakultät für Physik, Universität Duisburg-Essen, Lotharstr. 1, 47057 Duisburg, Germany

[a)] Martin@Mittendorff.email and Ryan.Suess@gmail.com

ABSTRACT

Black phosphorus possesses several attractive properties for optoelectronics, notably a direct and layer dependent bandgap that varies from the visible to mid-infrared and the ability to transfer the material to nearly arbitrary substrates. A less utilized property of black phosphorus for optoelectronics is the nonlinear photoresponse. The photocarrier lifetime in black phosphorus exhibits a strong nonlinear dependence on the excitation density that is utilized in the present work for optoelectronic mixing. In this scheme, two telecommunications-band lasers are intensity-modulated by a radio frequency (RF) and local oscillator (LO) frequency and focused onto a black phosphorus photoconductive detector. Above the saturation carrier density, the photocurrent is proportional to the square root of the optical power which produces photocurrents at the sum and difference frequencies of the input beams. The bandwidth of the mixing process increases from 10 to 100 MHz for incident powers of 0.01 to 1 mW, respectively. An excess carrier model accurately describes the power dependence of the cutoff frequency and mixing conversion, which are both limited by photocarrier recombination. Optimizing our device geometry to support larger bias fields and decreased carrier transit times could increase the maximum RF/LO frequency beyond a GHz by reducing the excess carrier lifetime. Frequency mixing based on the photocarrier nonlinearity in multilayer black phosphorus demonstrated here can be readily extended to mid-infrared wavelengths as long as 4 μm.

I. INTRODUCTION

Black phosphorus has generated interest as a versatile material for optoelectronics covering a large spectral range.[1–4] Similar to graphene and other 2D materials,[5,6] its layered structure allows for the mechanical exfoliation of atomically thin layers that can be transferred to substrates like SiO_2/Si, quartz, or even waveguides.[7,8] Flakes of different thicknesses feature a direct bandgap between the bulk value of 0.3 eV for thick flakes (more than 10 layers) to around 2 eV for single atomic layers.[9] While the single atomic layers are highly unstable under ambient conditions and will deteriorate without a protective layer in less than a minute, thicker flakes are more robust and can remain viable with a simple capping layer for many months.[10–12] Because of these favorable properties, black phosphorus has been employed as an active material for both detectors and modulators in the infrared range.[13–16] Black phosphorus also exhibits a photoconductive response that scales nonlinearly with applied optical power.[20] The origin of this nonlinearity is radiative carrier recombination, which results in decreased carrier collection efficiency as the applied optical power is increased. In the present work, we investigate the photocurrent nonlinearity in black phosphorus and demonstrate how it can be used for optoelectronic mixing. The nonlinear photocurrent of the black phosphorus photodetector is first studied over 5 orders of magnitude in optical power (10 nW to 1 mW) at a wavelength of 1.5 μm. The 3 dB cutoff frequency of our device is next measured with a network analyzer at varied optical powers and bias voltages. While the bias voltage shows no influence on the device bandwidth, the cutoff frequency is observed to shift from 10 MHz to 100 MHz with increasing optical power. We utilize this nonlinearity for the optoelectronic mixing of two independent laser sources that are modulated at frequencies of several hundred MHz and serve as radio frequency (RF) and local oscillator (LO) inputs to the mixer. At the electrical output, both RF and LO frequency, as well as sum and difference intermediate frequencies (IFs), are observed. The bandwidth of our device could potentially be extended beyond a GHz by shortening the black phosphorus channel and applying larger bias fields to sweep the carriers from the device.[21] The carrier nonlinearity utilized for mixing depends on the excited carrier density, indicating that the mixer presented here could be used at wavelengths as long as 4 μm due to the low bandgap of bulk black phosphorus.

II. EXPERIMENTAL DETAILS

A. Device fabrication and characterization

Device fabrication begins by exfoliating thin flakes (20-80 layers) of black phosphorus onto 300 nm thick SiO_2 on moderately doped Si (250 Ω cm). Photoresist is deposited onto the samples seconds after the material is transferred to the substrate. Electrical contacts to the flake are created using photolithography and subsequent deposition of 10 nm Cr and 100 nm Au. The electrical contacts define a 5 μm channel across the black phosphorus flake. Atomic-layer deposition is used to deposit a 100 nm capping layer of Al_2O_3 to allow for device operation in ambient conditions without degradation.[17] The total exposure of the flake to ambient conditions during fabrication is about 5 minutes. The flake used in this device is measured to be 80 layers (40 nm) using linear optical transmission measurements[20] and verified to be black phosphorus by identifying the characteristic Raman peaks at 364 cm^{-1}, 440 cm^{-1}, and 468 cm^{-1}.[1]

The optical response of the device is characterized using a variety of methods. Optical power and optical modulation frequency dependence measurements are carried out using a single continuous wave (CW) fiber-coupled diode laser with 1.5 μm wavelength that is modulated by using a Mach-Zehnder electrooptic modulator. Polarization controlling paddles are used in front of the modulator to ensure maximum coupling. The light is coupled to free space using a fiber collimator and focused onto the black phosphorus flake with an aspheric lens, achieving a diffraction limited spot of 5 μm. To maximize the photoconductive response, a half-wave plate is used to align the incident light along the high-mobility axis of the flake.[18,19] To carry out mixing measurements, two fiber-coupled CW diode lasers are used to illuminate the sample at wavelengths of 1.5 μm and 1.49 μm. Each of the lasers is connected to a Mach-Zehnder electrooptic modulator and combined with a 50/50 four-port fiber coupler. Polarization controlling paddles are used in front of the modulators as well as after one of the modulators to ensure maximum coupling efficiency and co-polarized beams. Two independent radio frequency sources are used to externally modulate the intensity of each laser at the RF and LO frequency. One of the two fiber coupler outputs is connected to an InGaAs photodiode for reference measurements, while the second output is coupled to free space and focused onto the device using the same method as described above. A sketch of the device and wiring is shown in Fig. 1(a).

B. Linearity measurement and excess carrier model

The strong photocurrent nonlinearity in black phosphorus has been found to match an excess carrier model with radiative recombination of the excited carriers.[20] Single beam, photocurrent linearity measurements are carried out over an intensity range of about 5 orders of magnitude in optical power. The electrooptic modulator is biased at quadrature and driven at high voltage to achieve 100% modulation depth at a frequency of 100 kHz before being coupled to free-space and focused onto the device as described above. The power for all reported measurements is controlled by varying the current supplied to the laser diode. For power values below 1 μW, a neutral density filter is inserted into the beam path to avoid instabilities close to the threshold of the laser diode.

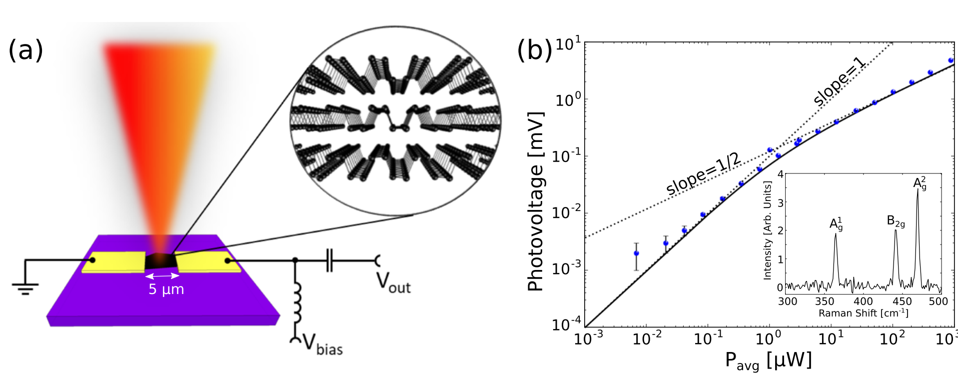

FIG. 1. (a) Diagram of the illuminated black phosphorus photoconductive detector and bias tee. Inset shows the multilayer black phosphorus structure. (b) Photovoltage as a function of the incident optical power for a single CW beam. The solid line is a fit from an excess carrier model. The inset shows the Raman spectrum of the black phosphorus flake used in the device.

All powers reported are incident average powers. The output of the detector is connected to a lock-in amplifier which measures the photovoltage shown in Fig. 1(b) via a bias tee. A bias voltage of 0.2 V is applied, leading to a dark current of 35.8 μA and device resistivity of 5.6 kΩ.

For average powers below 1.2 μW, the photovoltage is directly proportional to the incident power, with the lowest applied power of about 10 nW producing a photovoltage close to the noise floor of the measurement. In this linear range, the responsivity is around 20 mA/W, which is in the same range as comparable devices from other groups.[13,14] For average powers above 1.2 μW, the photovoltage is observed to be proportional to the square root of the incident power. This behavior can be explained by the density dependent excess carrier lifetime. In pulsed illumination measurements, such as pump-probe or autocorrelation measurements, a shorter carrier lifetime has been observed at pump intensities exceeding a saturation carrier density.[21] This effect is well described by an excess carrier model containing non-radiative and radiative recombination mechanisms having relative contributions of A (s^{-1}) and B ($cm^3\ s^{-1}$), respectively,

$$\frac{\partial \Delta n(t)}{\partial t} = G(t) - A\Delta n(t) - B\Delta n^2(t). \tag{1}$$

In this equation, $\Delta n(t)$ represents the excess photocarrier density and G(t) represents the time-dependent excess carrier generation. In our linearity measurement, the excess carrier density equation is solved in the steady-state condition $\partial\Delta n/\partial t$ for the case of CW illumination ($G(t) = const$),

$$\Delta n = \frac{1}{2} n_{sat}\left(\sqrt{1 + 4\frac{n_0}{n_{sat}}} - 1\right). \tag{2}$$

Here Δn is the steady state excess carrier density, $n_{sat} = A/B$ is the saturation density, and $n_0 = \eta I_{inc}/Ah\nu d$ is the photogenerated density where η, I_{inc}, A, $h\nu$, and d describe, respectively, the photon to electron conversion efficiency, incident intensity, non-radiative recombination coefficient, energy per photon (Planck constant times photon frequency), and sample thickness. The limit of Eq. (1) for $n_0/n_{sat} \ll 1$ and $\gg 1$ produces an excess density with a power dependence of one and one-half on the applied optical fluence, in agreement with the photosignal displayed in Fig. 1(b). By contrast, linearity measurements carried out with pulsed illumination exhibit an average signal with a logarithmic dependence on applied optical power.[20]

C. Bandwidth characterization

The cutoff frequency of our photoconductive device is determined by measuring the frequency dependent photocurrent produced by a single optical beam that is modulated over a range of frequencies. In this measurement, the output signal of a network analyzer is connected to the signal port of a Mach-Zehnder electrooptic modulator biased at quadrature with a modulation depth of 35%. The sinusoidal electrical signal applied to the modulator is imposed onto the intensity of the CW beam which is then coupled to free-space and focused onto the device. The output of the device is AC coupled to the input of the network analyzer via a bias tee, which is also used to apply a DC source-drain bias. A diagram of the cutoff frequency measurement is shown in Fig. 2(a). A reference measurement is performed with a high frequency InGaAs diode to account for the frequency dependence of the modulator, bias tee, and the cables. The measurements are repeated at various bias voltages and optical powers. Figure 2(b) shows the data taken at various bias voltages at a fixed optical power of 920 μW. The photocurrent increases linearly with the applied bias voltage as indicated by the 6 dB separation between detector response curves for each doubling of the bias. The cutoff frequency is observed to remain constant with bias voltage. By contrast, Youngblood and Li observed a shorter lifetime with increased bias field due to sweeping the photocarriers from the black phosphorus channel.[21] This difference is due to a shorter black phosphorus channel that has higher bias fields and therewith shorter carrier transit times. This indicates that further optimization of our device geometry could increase the cutoff frequency of our device. Figure 2(c) shows the results for different optical powers. For frequencies below 10 MHz, the response is flat, regardless of the optical power. At frequencies above 10 MHz, a decreased response is observed. While the cutoff frequency at the lowest power of 8 μW is around 10 MHz, it increases to nearly 100 MHz when the incident illumination has an average power of 920 μW. The increased cutoff frequency for higher optical powers matches the power dependent carrier lifetime predicted by Eq. (1) and is used to produce the dashed curves shown in Fig. 2(c). A carrier generation term of $G(t) = \frac{\eta I_{ac}}{dh\nu}(C + 1 - \cos(2\pi f t))$ is used in Eq. (1), where f represents the drive frequency from the network analyzer, I_{ac} is the amplitude of the modulation, and $C = I_{dc}/I_{ac}$ is the contrast of the modulation which is measured to be 0.15. Here I_{dc} represents the minimum intensity achieved from the modulation and results from partial switching of the modulator due to a voltage applied from the network analyzer that is less than the specified V_π of the modulator.

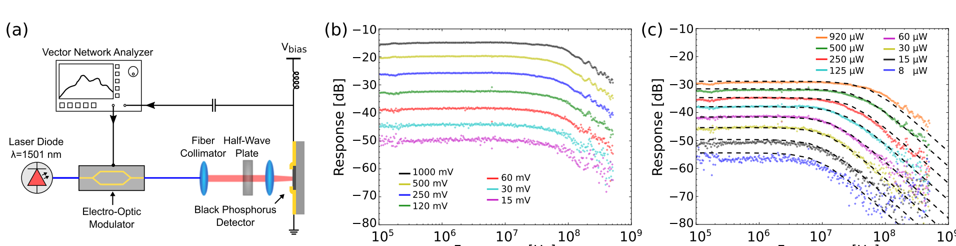

FIG. 2. (a) Diagram of frequency dependent photocurrent measurement. (b) The photocurrent as a function of the frequency is shown in (b) and (c) for different bias voltages and optical powers, respectively. The black lines in (c) denote calculations from the excess carrier model.

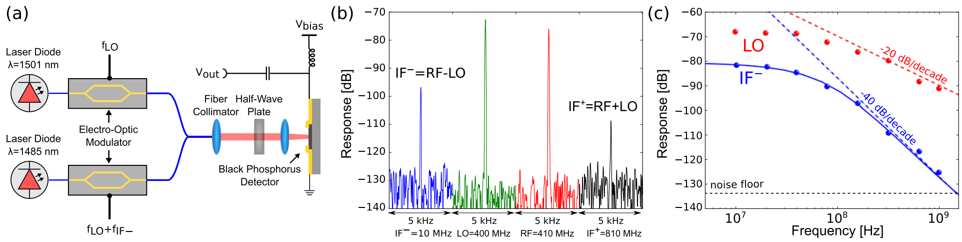

FIG. 3. (a) Diagram of mixing performance measurement. (b) Mixer output showing LO frequency, RF, and sum and difference frequencies for IF⁻ = 10 MHz. (c) Mixer output versus LO frequency with IF⁻ = 1 MHz. Solid curve is given by the excess carrier model.

In all model curves, A^{-1} is set to 22.5 ns and the applied saturation power to a value of 60 μW. As the minimum applied power used in the bandwidth measurements is 8 μW, we do not expect the estimated saturation power to reproduce the 1.2 μW obtained from the prior linearity measurement and instead treat this value as a phenomenological fit parameter. The model curves in Fig. 2(c) are directly proportional to the amplitude of the modulated excess carrier density at the drive frequency f and are determined by taking the Fourier transform of the time domain solution to Eq. (1). The agreement of the frequency response between the model and data shows that the cutoff frequency of our black-phosphorus device is determined by the excess carrier lifetime. This demonstrates that the bandwidth of our device can be extended by decreasing the carrier lifetime via the application of more optical power.

D. Frequency mixing demonstration

The nonlinear behavior observed in our device can be exploited for useful optical functions such as optoelectronic autocorrelation[22] and mixing.[23] For the case of optoelectronic autocorrelation, the electrical response time of the detector does not limit the temporal resolution of the response since the dynamics are measured with respect to the pulse delay between incident optical pulses. In the same way, the optoelectronic mixing allows the readout of a down-converted IF signal, even if the circuitry would be too slow for the incident high-frequency signals, since the mixing occurs in the black phosphorus, not in the electronics. To characterize the mixing performance of our device, we carried out measurements with two independently modulated lasers [cf. Fig. 3(a)]. One high-frequency signal generator served as the RF, while a second served as the LO. As the lasers for RF and LO frequency are modulated independently, there is no possibility of nonlinear mixing in the modulators. A voltage supply is used to bias the device via a bias tee. The high frequency output of the bias tee is connected to a spectrum analyzer. If only one of the lasers is activated, a signal at the corresponding frequency (LO frequency or RF) is observed (harmonics of this frequency are also visible). When both lasers are active simultaneously, a new signal appears at the intermediate frequency ($IF^- = RF - LO$), as well as at the sum frequency ($IF^+ = RF + LO$), as shown in Fig. 3(b). Both laser diodes are driven with identical currents, leading to an overall power of about 810 μW. A bias voltage of 0.2 V is applied to the black phosphorus device. The modulators are driven with an electrical power of 10 dBm to achieve a high modulation depth. For a LO frequency and RF of 20 MHz and 21 MHz, the power levels measured at the output of the device are −65 dBm and −69 dBm, respectively. At the IF^- of 1 MHz, as well as at the sum frequency of 41 MHz, an output power of −82 dBm is achieved. The frequency response of the device is measured by keeping the IF^- constant at 1 MHz but increasing RF and LO frequency up to 1 GHz. The output power of LO frequency and IF^- as a function of the modulation frequency is plotted in Fig. 3(c). For the LO signal, a cutoff frequency in the range of 100 MHz is observed, similar to the measurements performed with the network analyzer. The IF^- is observed to fall off with twice the slope of the LO frequency as it depends on the product of the RF and LO signals. The curve produced by the excess carrier model is shown as a solid line in the figure. Equation (1) is used with the source term set to $G(t) = \frac{\eta I_{ac}}{dh\nu}(2 - \cos(2\pi f_{LO}t) - \cos(2\pi f_{RF}t))$, where $f_{RF} = f_{LO} + f_{IF}$ and f_{IF} is set to 1 MHz. As was done for the cutoff frequency measurements, Eq. (1) is solved in the time domain and the Fourier components at the frequencies of interest were extracted. The model accurately describes the roll off for the IF^- with the slope being twice that of the LO frequency [cf. Fig. 3(c)], indicating that the excess carrier density radiative recombination model accurately describes both the mixing efficiency and bandwidth.

For real world applications, it is important that the device operates at low optical powers as would potentially be the case for a received signal in optical communications link. The low power performance of our device is investigated by reducing the optical power of both lasers to 30 μW each and reducing the RF and IF^- to 11 MHz and 1 MHz, respectively. This resulted in read out power values of −77 dBm, −80 dBm, and −98 dBm. Comparing these numbers to the ones measured at 810 μW, the difference between the RF and the IF^- power only slightly increases from 13 dB to 18 dB. The decreased mixing efficiency confirms that we are operating in a more linear region of the black phosphorus response curve [cf. Fig. 1]. Decreasing the power of the RF signal to −86 dBm (an incident optical power of around 3 μW) produces an IF^- of −106 dBm that is still well above the −144 dBm/Hz noise level of our measurement.

III. DISCUSSION

Optoelectronic mixing via a local oscillator applied directly to the active material of a nonlinear detector generally allows for the optimization of the detector design for the lower IF. For example, the first demonstration of optoelectronic down conversion was based on an AC biased photodiode: in addition to the DC bias, an electrical LO AC bias is applied to the photodiode, generating the IF.[25,26] This type of optoelectronic mixing is particularly interesting whenever a high frequency signal has to be received, as is the case for radio over fiber.[24] A similar method is to apply an electrical LO to a second, serially connected modulator, generating an optical IF before detection with a photodiode.[27] In another approach, exploiting the quadratic two-photon detection within the active material of a photodiode directly enables optoelectronic mixing.[28] A super-linear characteristic (as is the case for a diode) is not required for electrical IF generation as it was demonstrated recently in graphene using a sub-linear response.[23] As the photocurrent generation in graphene is linear over a large range, several tens of mW are required to reach a nonlinear regime that enables optoelectronic mixing. In contrast to graphene, the nonlinearity of photocurrent in our black phosphorus-based photodetector initiates at a very low optical power, which is consistent with earlier publications.[13,19] This strong nonlinearity, in combination with the versatility of a material that can be used on a wide variety of substrates, makes black phosphorus an extremely attractive material for optoelectronic mixing. The intrinsic speed of the device, which is determined by the photo-carrier lifetime, could be pushed to higher frequencies by applying a higher bias field that would sweep the carriers out of the black phosphorus faster than the radiative recombination time, potentially extending the bandwidth into the GHz range.[21] One barrier to achieving this in the current device is the relatively wide channel which is practically limited to 5 μm because of the resolution of the photolithographic patterning. A device fabricated using electron beam lithography would allow for narrower electrode geometries. For the same applied field, this will allow for shorter transit times and a greater ability to sweep out the carriers with an external voltage. Another method might be the manipulation of the black phosphorus itself. Ion implantation has been used to decrease the carrier lifetime in GaAs by two orders of magnitude[29] by introducing defect sites where free carriers can recombine. This approach thus offers a presently unexplored and potentially viable avenue for achieving GHz frequencies in black phosphorus-based devices.

We presented an experimental study of an optoelectronic mixer based on black phosphorus. The cutoff frequency of the device is in the range of 100 MHz and could readily be extended to the GHz range by optimizing the device geometry or potentially through modification of the black phosphorus via ion implantation techniques. In addition, the low bandgap of bulk black phosphorus flakes used in this study implies that the results presented here should extend to mid-infrared wavelengths as long as 4 μm. The low threshold of the nonlinear photocurrent generation already leads to a significant mixing at low optical powers in the μW range, making it suitable for optical communications applications. A model based on radiative recombination of the photoexcited carriers accurately describes the observed experimental results. The model further indicates that the mixing origin and bandwidth are due to carrier recombination mechanisms in the black phosphorus.

ACKNOWLEDGMENTS

Parts of this work were supported by the Office of Naval Research (ONR) Award No. N000141310865 and the National Science Foundation (NSF) Award No. ECCS1309750. The sample fabrication was carried out at the University of Maryland Nanocenter.

REFERENCES

[1] F. Xia, H. Wang, and Y. Jia, "Rediscovering black phosphorus as an anisotropic layered material for optoelectronics and electronics," Nat. Commun. **5**, 4458 (2014).
[2] A. Castellanos-Gomez, "Black phosphorus: Narrow gap, wide applications," J. Phys. Chem. Lett. **6**, 4280–4291 (2015).
[3] S. Huang and X. Ling, "Black phosphorus: Optical characterization, properties and applications," Small **13**, 1700823 (2017).
[4] X. Chen, X. Lu, B. Deng, O. Sinai, Y. Shao, C. Li, S. Yuan, V. Tran, K. Watanabe, T. Taniguchi, D. Naveh, L. Yang, and F. Xia, "Widely tunable black phosphorus mid-infrared photodetector," Nat. Commun. **8**, 1672 (2017).
[5] A. Castellanos-Gomez, "Why all the fuss about 2D semiconductors?," Nat. Photonics **10**, 202 (2016).
[6] F. Xia, H. Wang, D. Xiao, M. Dubey, and A. Ramasubramaniam, "Two-dimensional material nanophotonics," Nat. Photonics **8**, 899 (2014).
[7] S. P. Koenig, R. A. Doganov, H. Schmidt, A. H. C. Neto, and B. Özyilmaz, "Electric field effect in ultrathin black phosphorus," Appl. Phys. Lett. **104**, 103106 (2014).
[8] N. Youngblood and M. Li, "Integration of 2D materials on a silicon photonics platform for optoelectronics applications," Nanophotonics **6**, 1205–1218 (2017).
[9] V. Tran, R. Soklaski, Y. Liang, and L. Yang, "Layer-controlled band gap and anisotropic excitons in few-layer black phosphorus," Phys. Rev. B **89**, 235319 (2014).
[10] S. Gamage, A. Fali, N. Aghamiri, L. Yang, P. D. Ye, and Y. Abate, "Reliable passivation of black phosphorus by thin hybrid coating," Nanotechnology **28**, 265201 (2017).
[11] J. Na, K. Park, J. T. Kim, W. K. Choi, and Y.-W. Song, "Air-stable few-layer black phosphorus phototransistor for near-infrared detection," Nanotechnology **28**, 085201 (2017).
[12] B. Wan, B. Yang, Y. Wang, J. Zhang, Z. Zeng, Z. Liu, and W. Wang, "Enhanced stability of black phosphorus field-effect transistors with SiO_2 passivation," Nanotechnology **26**, 435702 (2015).
[13] M. Buscema, D. J. Groenendijk, S. I. Blanter, G. A. Steele, H. S. J. van der Zant, and A. Castellanos-Gomez, "Fast and broadband photoresponse of few-layer black phosphorus field-effect transistors," Nano Lett. **14**, 3347–3352 (2014).
[14] M. Engel, M. Steiner, and P. Avouris, "Black phosphorus photodetector for multispectral, high-resolution imaging," Nano Lett. **14**, 6414–6417 (2014).
[15] C. Chen, N. Youngblood, R. Peng, D. Yoo, D. A. Mohr, T. W. Johnson, S.-H. Oh, and M. Li, "Three-dimensional integration of black phosphorus photodetector with silicon photonics and nanoplasmonics," Nano Lett. **17**, 985–991 (2017).
[16] R. Peng, K. Khaliji, N. Youngblood, R. Grassi, T. Low, and M. Li, "Midinfrared electro-optic modulation in few-layer black phosphorus," Nano Lett. **17**, 6315–6320 (2017).
[17] J. D. Wood, S. A. Wells, D. Jariwala, K.-S. Chen, E. Cho, V. K. Sangwan, X. Liu, L. J. Lauhon, T. J. Marks, and M. C. Hersam, "Effective passivation of exfoliated black phosphorus transistors against ambient degradation," Nano Lett. **14**, 6964–6970 (2014).
[18] M. Baba, Y. Takeda, K. Shibata, T. Ikeda, and A. Morita, "Optical properties of black phosphorus and its application to the infrared detector," Jpn. J. Appl. Phys., Part 1 **28**, L2104 (1989).

[19]Q. Guo, A. Pospischil, M. Bhuiyan, H. Jiang, H. Tian, D. Farmer, B. Deng, C. Li, S.-J. Han, H. Wang, Q. Xia, T.-P. Ma, T. Mueller, and F. Xia, "Black phosphorus mid-infrared photodetectors with high gain," Nano Lett. **16**, 4648–4655 (2016).

[20]R. J. Suess, E. Leong, T. Zhou, R. Salem, T. E. Murphy, and M. Mittendorff, "Mid-infrared time resolved photoconduction in black phosphorus," 2D Mater. **3**, 041006 (2016).

[21]N. Youngblood and M. Li, "Ultrafast photocurrent measurements of a black phosphorus photodetector," Appl. Phys. Lett. **110**, 051102 (2017).

[22]M. Mittendorff, S. Winnerl, J. Kamann, J. Eroms, D. Weiss, H. Schneider, and M. Helm, "Ultrafast graphene-based broadband THz detector," Appl. Phys. Lett. **103**, 021113 (2013).

[23]C. Cheng, B. Huang, X. Mao, Z. Zhang, Z. Zhang, Z. Geng, P. Xue, and H. Chen, "Frequency conversion with nonlinear graphene photodetectors," Nanoscale **9**, 4082–4089 (2017).

[24]J. Capmany and D. Novak, "Microwave photonics combines two worlds," Nat. Photonics **1**, 319–330 (2007).

[25]Q. Z. Liu and R. I. MacDonald, "Controlled nonlinearity monolithic integrated optoelectronic mixing receiver," IEEE Photonics Technol. Lett. **5**, 1403–1406 (1993).

[26]A. Montanaro, S. Mzali, J.-P. Mazellier, O. Bezencenet, C. Larat, S. Molin, L. Morvan, P. Legagneux, D. Dolfi, B. Dlubak, P. Seneor, M.-B. Martin, S. Hofmann, J. Robertson, A. Centeno, and A. Zurutuza, "Thirty gigahertz optoelectronic mixing in chemical vapor deposited graphene," Nano Lett. **16**, 2988–2993 (2016).

[27]V. R. Pagán and T. E. Murphy, "Electro-optic millimeter-wave harmonic downconversion and vector demodulation using cascaded phase modulation and optical filtering," Opt. Lett. **40**, 2481–2484 (2015).

[28]R. Salem, A. A. Ahmadi, G. E. Tudury, G. M. Carter, and T. E. Murphy, "Two-photon absorption for optical clock recovery in OTDM networks," J. Lightwave Technol. **24**, 3353–3362 (2006).

[29]P. Deshmukh, M. Mendez-Aller, A. Singh, S. Pal, S. S. Prabhu, V. Nanal, R. G. Pillay, G. H. Döhler, and S. Preu, "Continuous wave terahertz radiation from antennas fabricated on C12-irradiated semi-insulating GaAs," Opt. Lett. **40**, 4540–4543 (2015).